THE JOURNAL OF PHYSICAL CHEMISTRY Letters

Letter

Cite This: J. Phys. Chem. Lett. 2019, 10, 6375−6381

pubs.acs.org/JPCL

Ordered Surface Nanostructures Self-Assembled from Rod−Coil Block Copolymers on Microspheres

Wenheng Xu,[†] Zhanwen Xu,[†] Chunhua Cai,* Jiaping Lin,* Shengmiao Zhang, Liangshun Zhang, Shaoliang Lin, Yuan Yao, and Huimin Qi

Shanghai Key Laboratory of Advanced Polymeric Materials, Key Laboratory for Ultrafine Materials of Ministry of Education, School of Materials Science and Engineering, East China University of Science and Technology, Shanghai 200237, China

Supporting Information

ABSTRACT: An ordered surface nanostructure endows materials advanced functions. However, fabricating ordered surface-patterned particles via the polymer self-assembly approach is a challenge. Here we report that poly(γ-benzyl-L-glutamate)-*block*-poly(ethylene glycol) rod−coil block copolymers are able to form uniform-surface micelles on polystyrene microspheres through a solution self-assembly approach. The size of the surface micelles can be varied by the molecular weight of the block copolymers. These surface micelles are arranged in a manner consistent with the Euler theorem. Most of the micelles are six-fold coordinated, and the number difference between the five-fold and the seven-fold coordination is 12. Simulations on model systems qualitatively reproduced the experimental findings and provided direct observations for the surface-patterned particles, including the polymer chain packing manner in surface micelles at the molecular level and the array feature of the surface micelles through 2D projections of the surface patterns.

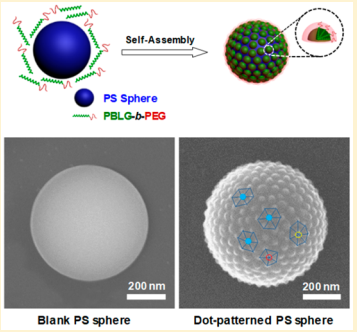

Ordered surface nanostructures of materials lead to unique and intriguing properties.[1−6] Particles with ordered surface nanostructures have attracted increasing attention recently.[7] Nature has provided an excellent example emphasizing the importance of the ordered surface nanostructure of particles. For example, viruses possess uniform surface nanostructures formed by proteins, and these proteins arrange in high order, which relates to their special functions, such as high cellular internalization efficiency.[8−10] Block copolymers (BCPs) are able to self-assemble into diverse nanostructures,[11−14] whereas on surface of microparticles they usually produce homogeneous films or irregular surface nanostructures.[7,15−18] There are very limited examples regarding BCP self-assembly into well-defined surface micelles on particulate substrates. In a recent work, Zhao et al. reported that poly(2-(dimethylamino)ethyl methacrylate)-*block*-polystyrene BCPs self-assemble into surface micelles on silica particles. These silica particles were grafted with polystyrene brushes, and the polystyrene brushes served as core-forming blocks for the surface micelles.[19] Although it has received considerable attention recently, the self-assembly of BCPs on particles into high-order surface nanostructures remains a challenge. In addition to the morphology of surface nanostructures, their array feature is another important structure characteristic for surface-patterned microparticles.[20−22] However, little is known about the arrangement characteristics of the surface nanostructures on particles.

Herein we report that poly(γ-benzyl-L-glutamate)-*block*-poly(ethylene glycol) (PBLG-*b*-PEG) rod−coil BCPs self-assemble into uniform and orderly arrayed surface micelles on the cross-linked polystyrene (PS) microspheres. Such surface-micelle-patterned microparticles exhibit some similarities to the hepatitis virus in structure and morphology (Scheme 1). The preparation process is as follows. First, the PBLG-*b*-PEG BCPs and PS microspheres were dissolved/dispersed in tetrahydrofuran/*N*,*N*′-dimethylformamide (THF/DMF) mixed solvents (3/7 v/v). Then, water was slowly added to the solution. Finally, through dialysis against water, an aqueous solution of the surface-micelle-patterned microparticles was obtained. In addition, dissipative particle dynamics (DPD) simulations on model systems were applied to gain deep insights into the inner structure and array feature of the surface micelles. In the following content, we first investigate the formation process and the structure of the surface micelles and then focus on the array features of the surface micelles.

The formation process was investigated by monitoring the surface morphology of the PS spheres under various water additions (Figure 1). The concentrations for BCPs and PS spheres were 0.125 and 0.375 g/L in the initial solution. As shown in Figure 1a, the scanning electron microscopy (SEM) image revealed that the PS spheres possess a smooth surface when mixed with the $PBLG_{29.5k}$-*b*-PEG_{5k} BCPs (the subscripts denote the number-average molecular weight, M_n, for each block) in the initial organic solvent. When 13.0 vol % water (i.e., the volume percentage of the added water relative to the whole volume) was added, the PS spheres exhibited a rough surface (Figure 1b), which indicates that the PBLG-*b*-PEG BCPs were adsorbed on PS spheres. The average thickness of

Received: September 5, 2019
Accepted: October 4, 2019
Published: October 4, 2019

DOI: 10.1021/acs.jpclett.9b02606
J. Phys. Chem. Lett. 2019, 10, 6375−6381

Scheme 1. Scheme of the Self-Assembly of PBLG-*b*-PEG Rod−Coil BCPs into Ordered Surface Micelles on PS Microspheres[a]

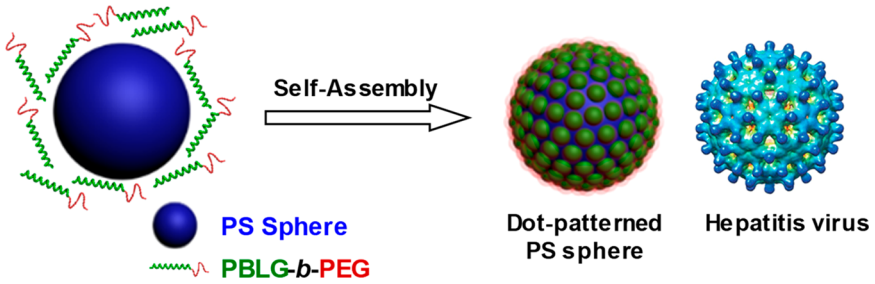

[a]Cartoon on the right shows the structure of a hepatitis virus. The blue sphere, green lines, and red lines represent the PS microsphere, PBLG blocks, and PEG blocks, respectively.

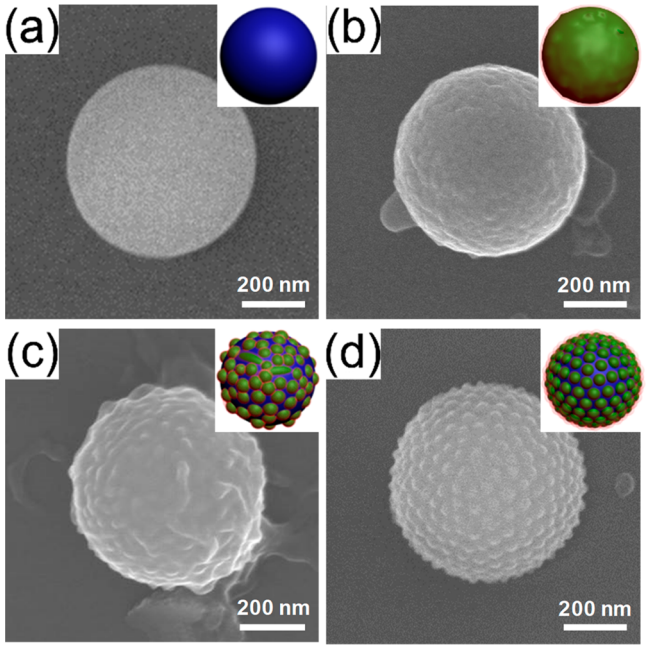

Figure 1. Morphology evolution of the surface nanostructures with the addition of water. (a−c) SEM images observed under various water contents: (a) 0, (b) 13.0, and (c) 28.6 vol %. No dialysis was performed before SEM observation in panels a−c. (d) After dialysis against water.

the BCP film on the PS spheres is ∼10.0 nm, which is obtained by comparing the diameter of the microparticles formed at 13.0% water (∼629.6 nm) and that of the original PS spheres (∼609.6 nm). When increasing the water content to 28.6 vol %, as shown in Figure 1c, a dot pattern on the surface of PS spheres appeared, which should be self-assembled from the BCPs. Note that for the samples observed in Figure 1a−c, no dialysis was performed before the SEM testing. Finally, after dialysis against water, the well-defined surface-micelle-patterned microparticles were obtained (Figure 1d). For these finally formed surface-patterned microparticles, the height of the surface micelles is ∼23 nm. (For details, see the later content.)

These observations suggested an adsorption−assembly process of the BCPs, including the adsorption of the PBLG-*b*-PEG BCPs on PS spheres and the subsequent assembly of the BCPs into surface micelles. In the THF/DMF mixed solvents, the PBLG-*b*-PEG BCPs are well dissolved, and the PS spheres can be homogeneously dispersed under stirring. (Both THF and DMF are good solvents for the PBLG, PEG, and PS segments.) With the addition of water, because of the hydrophobicity of the PBLG and PS segments, the BCPs tend to attach on the surface of the PS spheres to lower the contact of both the PS microspheres and the PBLG blocks with water. Additionally, the $\pi-\pi$ attractions between PBLG−PS pairs could enhance the stability of the BCP/PS sphere assemblies in solution.[23,24] Because of the rigid nature of the PBLG segments,[25] the PBLG-*b*-PEG BCPs could lie down on surface of the spheres, and the surface film contains a multilayer of the BCPs. When more water is added, the adsorbed BCPs self-assemble into surface micelles (PBLG as the core and PEG as the corona) to further reduce the contact of the PBLG blocks with water.

Importantly, the rod−coil nature of the PBLG-*b*-PEG BCPs is essential for preparing such surface micelles. (PBLG is a rod polymer that has a persistence length up to 200 nm.[25]). Because PS is a flexible polymer[25,26] and the interaction between PBLG−PS pairs is comparable to that between PS−PS pairs,[27,28] we replaced the PBLG-*b*-PEG rod−coil BCPs with PS-*b*-PEG coil−coil BCPs to cooperatively assemble with the PS spheres under similar conditions. Three PS-*b*-PEG BCPs with the same PEG blocks and various PS block lengths, that is, $PS_{10.3k}$-*b*-PEG_{5k}, $PS_{15.5k}$-*b*-PEG_{5k}, and $PS_{30.2k}$-*b*-PEG_{5k}, were used in the studies. It was found that the PS spheres can be stabilized by the PS-*b*-PEG BCPs in water, but a rough surface instead of ordered surface micelles was formed on the PS spheres. (See Figure S3 in the Supporting Information.) The PS-*b*-PEG coil−coil BCPs could form a polymer brush on the spheres, with the PS blocks attached to the surface and the PEG blocks stretching into the solvent.[29,30] These results indicated the importance of the rod−coil nature of the building BCPs for the construction of uniform surface micelles.

Typical morphologies of the microparticles were characterized by SEM and atomic force microscopy (AFM) analyses (Figure 2). As shown in Figure 2a, bare PS microspheres have a smooth surface, and their diameter is uniform (∼609 nm). After self-assembling with $PBLG_{29.5k}$-*b*-PEG_{5k} BCPs, the microparticles are fully covered by uniform dot-like surface micelles (Figure 2b). The distance between the neighboring surface micelles (corresponding to the diameter of the surface micelles) is ∼55 nm. AFM testing gives a similar average diameter value of the surface micelles (Figure 2e). The height of the surface micelles was indirectly obtained by comparing the size of the PS microparticles before and after assembling with the BCPs (Figure S4). For the $PBLG_{29.5k}$-*b*-PEG_{5k} surface micelles, the height is estimated to be 23 nm. Because the height is close to half of their diameter, these dot-like surface micelles are inferred as hemispherical micelles.[31,32]

DOI: 10.1021/acs.jpclett.9b02606
J. Phys. Chem. Lett. 2019, 10, 6375−6381

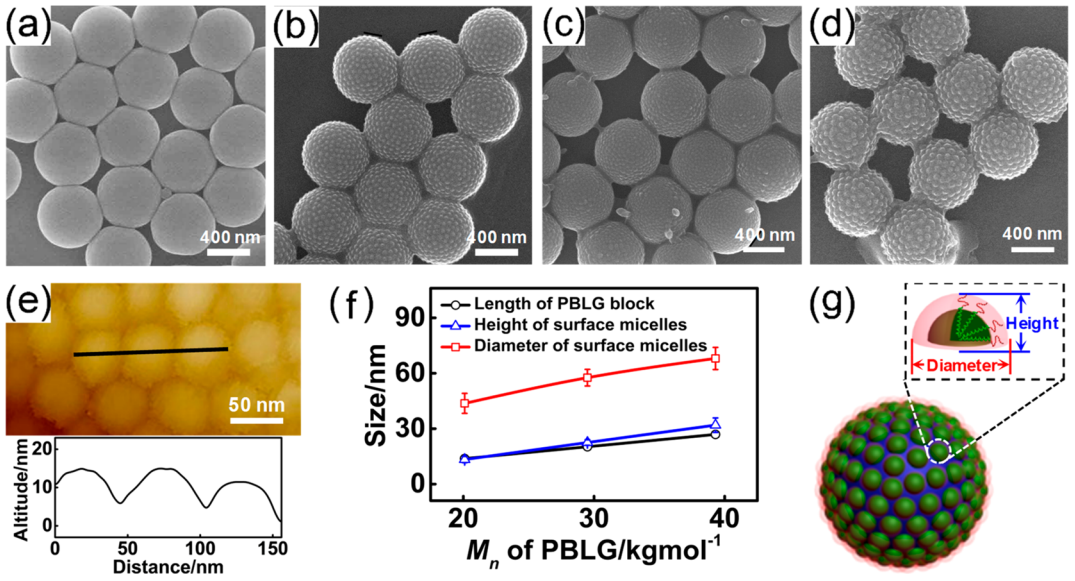

Figure 2. Morphology and structure of the surface micelles. (a) SEM images of original PS spheres. (b–d) SEM images of particles with dot-like surface nanostructures self-assembled from (b) $PBLG_{29.5k}$-*b*-PEG_{5k} BCPs, (c) $PBLG_{20.1k}$-*b*-PEG_{5k} BCPs, and (d) $PBLG_{39.3k}$-*b*-PEG_{5k} BCPs, respectively. (e) AFM image and the height profile of the particles shown in panel b. (f) Plots of the length of the PBLG block versus the diameter and height of the surface micelles formed by various PBLG-*b*-PEG BCPs. (g) Scheme of the structure of the surface micelles.

The size of the surface micelles can be regulated by M_n of the PBLG blocks. As can be seen from Figure 2c,d, both $PBLG_{20.1k}$-*b*-PEG_{5k} and $PBLG_{39.3k}$-*b*-PEG_{5k} BCPs form uniform surface micelles, and they fully cover the PS microspheres. As shown in Figure 2f, it was found that the diameter of the surface micelles increases approximately linearly with the M_n value of the PBLG blocks, that is, from ~43 (M_n of the PBLG block is 20.1 kg·mol^{-1}) to ~55 nm (M_n of the PBLG block is 29.5 kg·mol^{-1}) and then to ~67 nm (M_n of the PBLG block is 39.3 kg·mol^{-1}). Simultaneously, the height of the surface micelles also increases with the M_n value of the PBLG blocks and retains about half of their diameter (Figure 2f). However, when the M_n value of the PBLG block is much smaller (e.g., M_n = 15.3 kg·mol^{-1}) or much larger (e.g., M_n = 61.5 kg·mol^{-1}), no ordered surface nanostructures are obtained. Details regarding the effect of the M_n value of the PBLG blocks on the surface morphology and the size of the surface micelles can be found in the Supporting Information (Figure S5).

Because of the rigid nature of the PBLG blocks, their length can be calculated from their molecular weights.[33] For example, the PBLG block with M_n = 29.5 kg·mol^{-1} has a length of ~20.2 nm. By analyzing the relationship between the diameter of the surface micelles and the length of the PBLG blocks, a head-to-head packing mode of the BCPs in the surface micelles is deduced (Figure 2g).[34−36] For the surface micelles, the hydrophobic PBLG blocks form the core, and the hydrophilic PEG chains form the corona extending to the solution.

We then analyzed array features of these surface micelles. It is well known that on a flat substrate spherical particles could arrange into a simple lattice of triangles, which prefer to form six-fold coordinated lattices,[37−41] whereas on a curved surface, other array modes, typically five-fold and seven-fold coordinated lattices, should exist. The five-fold and seven-fold coordinated lattices are characterized by +1 and −1 disclinations, respectively. On the basis of the Euler theorem, for ordered packed lattices on spheres with an ideal array mode, the total excess disclinations (the difference in numbers between +1 disclinations and −1 disclinations) are +12.[38,40] For the present systems, as shown in Figure 3a,e,f, the array types of the surface micelles, including six-fold coordinated, five-fold coordinated, and seven-fold coordinated, are discerned. Figure 3b–d shows enlarged images for these array types, respectively.

Because SEM images reflect only the top side of the spheres, an extrapolation method was used to deduce the total number of surface micelles on a sphere. For example, Figure 3a shows a limited area delineated by a black circle accounting for ~19.2% of the total area. (See Figure S6 in the Supporting Information.) The number of surface micelles in this area can be counted, and the total number of surface micelles on one sphere can be obtained by extrapolating this number to the whole sphere surface. Analysis results revealed that the average number of surface micelles formed by $PBLG_{20.1k}$-*b*-PEG_{5k}, $PBLG_{29.5k}$-*b*-PEG_{5k}, and $PBLG_{39.3k}$-*b*-PEG_{5k} BCPs is 544, 362, and 242, respectively.

The array feature analysis revealed that the six-fold coordination is the majority array type for the surface micelles in all of the systems, and the total excess disclinations for these systems are in the range of 12.5 to 13.5, which are close to the theoretical value of 12. These results indicated that the surface micelles on the microspheres packed in high order. The details regarding the arrangement of the surface micelles formed by various BCPs are summarized in Table 1.

In addition to the array features of the surface micelles, the dislocation structure is also analyzed. It is well known that seven-fold coordinated surface micelles are always tightly bound to five-fold coordinated surface micelles, forming a dislocation, which is also clearly observed in the present system. The 5−7 pair dislocations usually form a chain of 5−7−5−7−...−5, which is called a scar. As shown in Figure 3, several scars are observed, and their length increases with a decrease in the M_n of the PBLG blocks (corresponding to increases in the number of surface micelles). These observations are consistent with the theory that increasing the number of particles on the spherical surface will introduce

DOI: 10.1021/acs.jpclett.9b02606
J. Phys. Chem. Lett. 2019, 10, 6375−6381

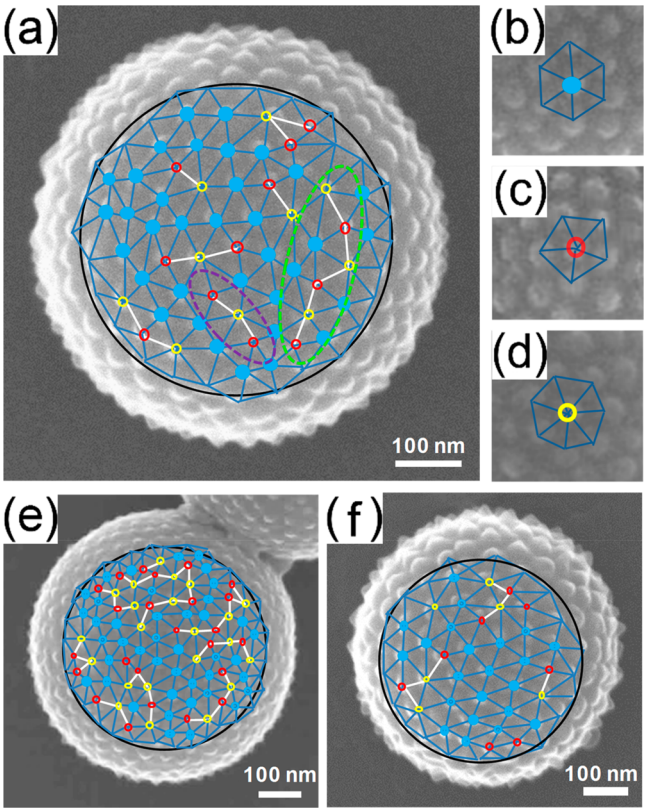

Figure 3. Array feature analysis of the surface micelles formed by PBLG-*b*-PEG BCPs with various M_n values of the PBLG blocks. (a) M_n = 29.5 kg·mol^{-1}. (b–d) Enlarged views of six-, five-, and seven-fold coordinated hemispherical micelles, respectively. (e) M_n = 20.1 kg·mol^{-1}. (f) M_n = 39.3 kg·mol^{-1}. The small blue dots and red and yellow circles represent six-, five-, and seven-fold coordinated hemispherical micelles, respectively. Typical scars and pleats are indicated by purple and green dashed ovals, respectively.

more scars to balance the configuration of surface defects on the spheres.[38] Besides the 5–7–5–7–...–5 chains (scars), some 5–7–5–7–...–7 chains, namely, pleats are also observed. Pleats are an interesting dislocation structure, which, unlike the scars, possess zero topological charge. The existence of pleats has no effect on the total excess disclinations but lowers the ordering of the surface patterns. Usually, pleats are observed on surfaces with a negative Gaussian curvature.[42] For the present system, the formation of pleats could be attributed to the uneven surface of the PS microspheres. (See Figure S2 in the Supporting Information.) Additionally, more pleats are formed by the BCPs with shorter PBLG blocks (Figure 3e). This phenomenon should be related to the smaller diameter of the surface micelles, which makes them more sensitive to the uneven parts of the surface of the PS spheres.

To support the experimental findings, coarse-grained DPD simulations are used to examine the self-assembly behaviors.[14,43] A model consisting of rod–coil BCPs (R_6C_5) and cross-linked homopolymer spheres (P) was constructed (Figure 4a). The R segments representing the PBLG blocks are hydrophobic and rigid, and the hydrophilic and flexible C segments represent the PEG blocks. In the model of the homopolymer sphere, cross-linking was created by generating random covalent bonds between neighboring homopolymer chains, and the diameter of the sphere was ~56r_c. (r_c is the cutoff distance in DPD simulations.) The interaction parameter between the R blocks and the sphere (a_{RP}) was set as 25 to guarantee the adsorption of the RC BCPs on the spheres. Accordingly, the interaction parameter between the rod block and the solvent (a_{RS}) was set to 70. The self-assembled structures in the simulations were collected after the system reached the steady state. Details of the simulation methods and parameter settings can be found in the Supporting Information (Section 10).

As shown in Figure 4b, the simulations revealed that spherical surface micelles were formed by R_6C_5 BCPs on the surface of the sphere. The cross-sectional images revealed that these surface micelles have a hemispherical structure (Figure 4c). Furthermore, as seen in Figure 4d, the R blocks in the core of the surface micelles arrange in a head-to-head manner, and the C blocks extend outside the core and form the shell. These simulations prove the models we proposed from the experimental observations. The effect of the rod block length of the RC BCPs on surface nanostructures was studied (Figure S8). To model a change in the molecular weight of the PBLG-*b*-PEG BCPs, the number of R beads was changed from 5 to 7, and the number of C beads was set to 5. It was found that with an increase in the bead number of the R block from 5 to 7, the diameter of the surface micelles increases, and the number of surface micelles on the sphere decreases, which is consistent with the experimental studies.

The array features of the surface micelles formed by the model rod–coil BCPs were then analyzed. To make clear observations, a Winkel Tripel projection of spheres with surface micelles was plotted (Figure 4e).[44] As can be seen, the majority of the surface micelles were six-fold coordinated, and five-fold and seven-fold coordinated surface micelles were also observed. By counting all of the coordinated lattices, we found that the total excess disclination number is 12, which is consistent with the theoretical value. In addition, scars (5–7...7–5 chains) were observed, but no pleats were found. The absence of pleats could be due to the smooth surface of the sphere built in the simulations, whereas pleats are usually

Table 1. Array Features of Surface Micelles Formed by PBLG-*b*-PEG BCPs with Various M_n Values of the PBLG Block

		six-fold coordinated surface micelles		five-fold coordinated surface micelles (+1 disclination)		seven-fold coordinated surface micelles (−1 disclination)		
M_n of PBLG (kg·mol^{-1})	number of the surface micelles on each sphere	number	%	number	%	number	%	total excess disclination number
20.1	544.5 ± 15.3	256.6	47.1	150.2	27.5	137.7	25.3	12.5
29.5	361.9 ± 12.5	222.2	61.4	76.2	21.1	63.5	17.5	12.7
39.3	242.0 ± 11.0	147.9	61.1	53.8	22.2	40.3	16.7	13.5

DOI: 10.1021/acs.jpclett.9b02606
J. Phys. Chem. Lett. 2019, 10, 6375–6381

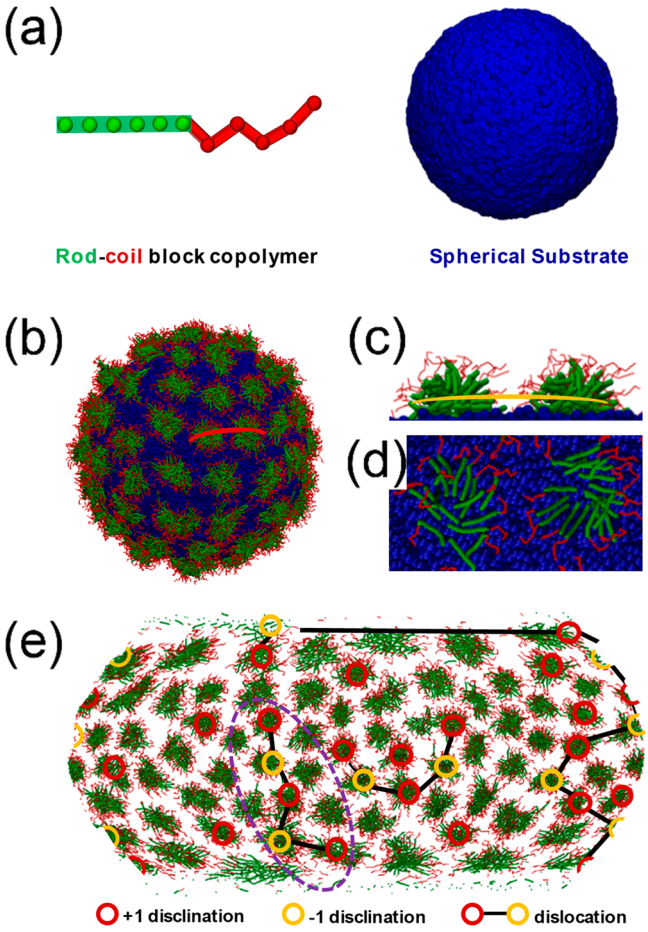

Figure 4. DPD simulations for the structure and array features of the surface micelles formed by model rod−coil BCPs on the microsphere. (a) DPD model of the R_6C_5 rod−coil BCP and the homopolymer sphere ($56r_c$, where r_c is the cutoff distance in DPD simulations). The rod and coil blocks and the microsphere are colored green, red, and blue, respectively. (b) Simulation prediction of a microsphere covered with surface micelles formed by R_6C_5 rod−coil BCPs. (c) Cross-sectional image of the surface micelles along the red line in panel b. (d) Cross-sectional image of the surface micelles along the yellow line in panel c. (e) Winkel Tripel projection of the surface micelle pattern in panel b. The purple dashed oval indicates a scar (a 5−7−5−7−5 chain). Solvents are not shown in all of these panels.

generated on a surface with a negative Gaussian curvature. For the surface micelles formed by R_5C_5 and R_7C_5, they possess similar array features, and the total excess disclination number remains 12 (Figure S8). The simulation results qualitatively reproduce the experimental observations for the array feature of the surface micelles, which confirm the highly ordered arrays of the surface micelles in experiment.

In summary, we demonstrated that PBLG-*b*-PEG rod−coil BCPs are capable of assembling into uniform surface micelles with a high-order arrangement on microparticles. The structures and array features of the surface micelles were explored by a combination of experiments and simulations. The sizes of the surface micelles are uniform and can be controlled by the molecular weight of the BCPs. The arrangement of the surface micelles obeys the Euler theorem; that is, the majority arrangement of the surface micelles is six-fold coordination, and the excess disclination number is 12. These prepared surface-patterned microparticles could find an application in the following fields. (1) These core−shell microparticles with ordered surface nanostructures show some similarities to the natural virus in the surface morphology, which could enable them to be models for the natural virus.[5,45] (2) The surface micelles, a kind of Janus nanoparticle (one side comprises hydrophilic PEG chains and the other side is hydrophobic PBLG chains), could serve as nanosurfactants when they are exfoliated from the microparticles.[46,47] (3) Furthermore, the terminating chains of 5−7 pair dislocations (both scars and pleats) could act as chemical reaction sites or initiation sites of bacterial cell division.[37,48] This work expands the research scope of BCP self-assembly, and the information gained could guide the fabrication of materials with highly ordered surface nanostructures.

■ ASSOCIATED CONTENT

Supporting Information

The Supporting Information is available free of charge on the ACS Publications website at DOI: 10.1021/acs.jpclett.9b02606.

Full experimental details including the synthesis and characterization of copolymers and microspheres, the aggregate preparation, influencing factors for surface nanostructures, the analysis method for the array feature of surface micelles, and the DPD simulation (PDF)

■ AUTHOR INFORMATION

Corresponding Authors

*E-mail: caichunhua@ecust.edu.cn (C.C.).
*E-mail: jlin@ecust.edu.cn (J.L.).

ORCID

Chunhua Cai: 0000-0001-9008-6327
Jiaping Lin: 0000-0001-9633-4483
Shengmiao Zhang: 0000-0002-6859-2538
Liangshun Zhang: 0000-0002-0182-7486
Shaoliang Lin: 0000-0003-3374-9934
Yuan Yao: 0000-0001-9959-4707
Huimin Qi: 0000-0003-4742-2561

Author Contributions

†W.X. and Z.X. contributed equally to this work.

Notes

The authors declare no competing financial interest.

■ ACKNOWLEDGMENTS

This work was supported by the National Natural Science Foundation of China (51573049, 51833003, 51621002, and 21975073).

■ REFERENCES

(1) Verma, A.; Uzun, O.; Hu, Y.; Hu, Y.; Han, H. S.; Watson, N.; Chen, S.; Irvine, D. J.; Stellacci, F. Surface-Structure-Regulated Cell-Membrane Penetration by Monolayer-Protected Nanoparticles. *Nat. Mater.* **2008**, *7*, 588−595.

(2) Jackson, A. M.; Myerson, J. W.; Stellacci, F. Spontaneous Assembly of Subnanometre-Ordered Domains in the Ligand Shell of Monolayer-Protected Nanoparticles. *Nat. Mater.* **2004**, *3*, 330−336.

(3) Sagawa, T.; Yoshikawa, S.; Imahori, H. One-Dimensional Nanostructured Semiconducting Materials for Organic Photovoltaics. *J. Phys. Chem. Lett.* **2010**, *1*, 1020−1025.

(4) Li, F.; Hou, H.; Yin, J.; Jiang, X. Near-Infrared Light-Responsive Dynamic Wrinkle Patterns. *Sci. Adv.* **2018**, *4*, No. eaar5762.

(5) Xue, J.; Guan, Z.; Lin, J.; Cai, C.; Zhang, W.; Jiang, X. Cellular Internalization of Rod-Like Nanoparticles with Various Surface

DOI: 10.1021/acs.jpclett.9b02606
J. Phys. Chem. Lett. 2019, 10, 6375−6381

Patterns: Novel Entry Pathway and Controllable Uptake Capacity. *Small* **2017**, *13*, 1604214.
(6) Li, C. Y.; Li, L.; Cai, W.; Kodjie, S. L.; Tenneti, K. K. Nanohybrid Shish-Kebabs: Periodically Functionalized Carbon Nanotubes. *Adv. Mater.* **2005**, *17*, 1198−1202.
(7) Liu, Y.; Goebl, J.; Yin, Y. Templated Synthesis of Nanostructured Materials. *Chem. Soc. Rev.* **2013**, *42*, 2610−2653.
(8) Böttcher, B.; Wynne, S.; Crowther, R. Determination of the Fold of the Core Protein of Hepatitis B Virus by Electron Cryomicroscopy. *Nature* **1997**, *386*, 88−91.
(9) Hamblin, M. N.; Xuan, J.; Maynes, D.; Tolley, H. D.; Belnap, D. M.; Woolley, A. T.; Lee, M. L.; Hawkins, A. R. Selective Trapping and Concentration of Nanoparticles and Viruses in Dual-Height Nanofluidic Channels. *Lab Chip* **2010**, *10*, 173−178.
(10) Lutomski, C. A.; Lyktey, N. A.; Zhao, Z.; Pierson, E. E.; Zlotnick, A.; Jarrold, M. F. Hepatitis B Virus Capsid Completion Occurs Through Error Correction. *J. Am. Chem. Soc.* **2017**, *139*, 16932−16938.
(11) Mai, Y.; Eisenberg, A. Self-Assembly of Block Copolymers. *Chem. Soc. Rev.* **2012**, *41*, 5969−5985.
(12) Orilall, M. C.; Wiesner, U. Block Copolymer Based Composition and Morphology Control in Nanostructured Hybrid Materials for Energy Conversion and Storage: Solar Cells, Batteries, and Fuel Cells. *Chem. Soc. Rev.* **2011**, *40*, 520−535.
(13) Kemling, J. W.; Qavi, A. J.; Bailey, R. C.; Suslick, K. S. Nanostructured Substrates for Optical Sensing. *J. Phys. Chem. Lett.* **2011**, *2*, 2934−2944.
(14) Zhang, Q.; Lin, J.; Wang, L.; Xu, Z. Theoretical Modeling and Simulations of Self-Assembly of Copolymers in Solution. *Prog. Polym. Sci.* **2017**, *75*, 1−30.
(15) Caruso, F.; Lichtenfeld, H.; Donath, E.; Möhwald, H. Investigation of Electrostatic Interactions in Polyelectrolyte Multilayer Films: Binding of Anionic Fluorescent Probes to Layers Assembled onto Colloids. *Macromolecules* **1999**, *32*, 2317−2328.
(16) Mandal, T. K.; Fleming, M. S.; Walt, D. R. Production of Hollow Polymeric Microspheres by Surface-Confined Living Radical Polymerization on Silica Templates. *Chem. Mater.* **2000**, *12*, 3481−3487.
(17) Goldmann, A. S.; Walther, A.; Nebhani, L.; Joso, R.; Ernst, D.; Loos, K.; Barner-Kowollik, C.; Barner, L.; Müller, A. H. E. Surface Modification of Poly(divinylbenzene) Microspheres via Thiolene Chemistry and Alkyne-Azide Click Reactions. *Macromolecules* **2009**, *42*, 3707−3714.
(18) Jia, L.; Tong, L.; Liang, Y.; Petretic, A.; Guerin, G.; Manners, I.; Winnik, M. A. Templated Fabrication of Fiber-Basket Polymersomes via Crystallization-Driven Block Copolymer Self-Assembly. *J. Am. Chem. Soc.* **2014**, *136*, 16676−16682.
(19) Hou, W.; Feng, Y.; Li, B.; Zhao, H. Coassembly of Linear Diblock Copolymer Chains and Homopolymer Brushes on Silica Particles: A Combined Computer Simulation and Experimental Study. *Macromolecules* **2018**, *51*, 1894−1904.
(20) Stoop, N.; Dunkel, J. Defect Formation Dynamics in Curved Elastic Surface Crystals. *Soft Matter* **2018**, *14*, 2329−2338.
(21) Yazyev, O. V.; Helm, L. Defect-Induced Magnetism in Graphene. *Phys. Rev. B: Condens. Matter Mater. Phys.* **2007**, *75*, 125408.
(22) Dodgson, M. J. W.; Moore, M. A. Vortices in a Thin-Film Superconductor with a Spherical Geometry. *Phys. Rev. B: Condens. Matter Mater. Phys.* **1997**, *55*, 3816.
(23) Kuo, S. W.; Chen, C. J. Functional Polystyrene Derivatives Influence the Miscibility and Helical Peptide Secondary Structures of Poly(γ-benzyl L-glutamate). *Macromolecules* **2012**, *45*, 2442−2452.
(24) Zhang, S.; Cai, C.; Huang, Q.; Lin, J.; Xu, Z. Effect of Intermolecular Interactions on Self-assembled Structures of Polypeptide-Based Copolymer/Polystyrene Derivatives Blends. *Acta Polym. Sin.* **2018**, 109−118.
(25) Rosales, A. M.; Murnen, H. K.; Kline, S. R.; Zuckermann, R. N.; Segalman, R. A. Determination of the Persistence Length of Helical and Non-Helical Polypeptoids in Solution. *Soft Matter* **2012**, *8*, 3673−3680.
(26) Nakajima, K.; Watabe, H.; Nishi, T. Single Polymer Chain Rubber Elasticity Investigated by Atomic Force Microscopy. *Polymer* **2006**, *47*, 2505−2510.
(27) Cai, C.; Li, Y.; Lin, J.; Wang, L.; Lin, S.; Wang, X. S.; Jiang, T. Simulation-Assisted Self-Assembly of Multicomponent Polymers into Hierarchical Assemblies with Varied Morphologies. *Angew. Chem., Int. Ed.* **2013**, *52*, 7732−7736.
(28) Kim, K. T.; Park, C.; Vandermeulen, G. W.; Rider, D. A.; Kim, C.; Winnik, M. A.; Manners, I. Gelation of Helical Polypeptide-Random Coil Diblock Copolymers by a Nanoribbon Mechanism. *Angew. Chem., Int. Ed.* **2005**, *44*, 7964−7968.
(29) Schneck, E.; Schollier, A.; Halperin, A.; Moulin, M.; Haertlein, M.; Sferrazza, M.; Fragneto, G. Neutron Reflectometry Elucidates Density Profiles of Deuterated Proteins Adsorbed onto Surfaces Displaying poly (Ethylene Glycol) Brushes: Evidence for Primary Adsorption. *Langmuir* **2013**, *29*, 14178−14187.
(30) Marques, C.; Joanny, J. F.; Leibler, L. Adsorption of Block Copolymers in Selective Solvents. *Macromolecules* **1988**, *21*, 1051−1059.
(31) Han, Y.; Cai, C.; Lin, J.; Gong, S.; Xu, W.; Hu, R. Self-Assembly of Rod-Coil Block Copolymers on Carbon Nanotubes: A Route toward Diverse Surface Nanostructures. *Macromol. Rapid Commun.* **2018**, *39*, 1800080.
(32) Warr, G. G. Surfactant Adsorbed Layer Structure at Solid/Solution Interfaces: Impact and Implications of AFM Imaging Studies. *Curr. Opin. Colloid Interface Sci.* **2000**, *5*, 88−94.
(33) Ding, W.; Lin, S.; Lin, J.; Zhang, L. Effect of Chain Conformational Change on Micelle Structures: Experimental Studies and Molecular Dynamics Simulations. *J. Phys. Chem. B* **2008**, *112*, 776−783.
(34) Lee, M.; Cho, B.-K.; Zin, W.-C. Supramolecular Structures from Rod-Coil Block Copolymers. *Chem. Rev.* **2001**, *101*, 3869−3892.
(35) Lim, Y.-b.; Moon, K.-S.; Lee, M. Rod-Coil Block Molecules: Their Aqueous Self-Assembly and Biomaterials Applications. *J. Mater. Chem.* **2008**, *18*, 2909−2918.
(36) Olsen, B. D.; Segalman, R. A. Self-Assembly of Rod−Coil Block Copolymers. *Mater. Sci. Eng., R* **2008**, *62*, 37−66.
(37) Bausch, A. R.; Bowick, M. J.; Cacciuto, A.; Dinsmore, A. D.; Hsu, M. F.; Nelson, D. R.; Nikolaides, M. G.; Travesset, A.; Weitz, D. A. Grain Boundary Scars and Spherical Crystallography. *Science* **2003**, *299*, 1716−1718.
(38) Tang, P.; Qiu, F.; Zhang, H.; Yang, Y. Phase Separation Patterns for Diblock Copolymers on Spherical Surfaces: A Finite Volume Method. *Phys. Rev. E* **2005**, *72*, 016710.
(39) Pérez-Garrido, A.; Moore, M. A. Symmetric Patterns of Dislocations in Thomson's Problem. *Phys. Rev. B: Condens. Matter Mater. Phys.* **1999**, *60*, 15628−15631.
(40) Zhang, L.; Wang, L.; Lin, J. Defect Structures and Ordering Behaviours of Diblock Copolymers Self-Assembling on Spherical Substrates. *Soft Matter* **2014**, *10*, 6713−6721.
(41) Kohyama, T.; Gompper, G. Defect Scars on Flexible Surfaces with Crystalline Order. *Phys. Rev. Lett.* **2007**, *98*, 198101.
(42) Irvine, W. T.; Vitelli, V.; Chaikin, P. M. Pleats in Crystals on Curved Surfaces. *Nature* **2010**, *468*, 947−951.
(43) Zhuang, Z.; Jiang, T.; Lin, J.; Gao, L.; Yang, C.; Wang, L.; Cai, C. Hierarchical Nanowires Synthesized by Supramolecular Stepwise Polymerization. *Angew. Chem., Int. Ed.* **2016**, *55*, 12522−12527.
(44) Chew, L. P. Constrained Delaunay Triangulations. *Algorithmica* **1989**, *4*, 97−108.
(45) Wang, J. C.; Mukhopadhyay, S.; Zlotnick, A. Geometric Defects and Icosahedral Viruses. *Viruses* **2018**, *10*, 25.
(46) Shin, H. I.; Min, B. G.; Jeong, W.; Park, C. Amphiphilic Block Copolymer Micelles: New Dispersant for Single Wall Carbon Nanotubes. *Macromol. Rapid Commun.* **2005**, *26*, 1451−1457.
(47) Gröschel, A. H.; Löbling, T. I.; Petrov, P. D.; Müllner, M.; Kuttner, C.; Wieberger, F.; Müller, A. H. Janus Micelles as Effective

DOI: 10.1021/acs.jpclett.9b02606
J. Phys. Chem. Lett. 2019, 10, 6375−6381

Supracolloidal Dispersants for Carbon Nanotubes. *Angew. Chem., Int. Ed.* **2013**, *52*, 3602−3606.
(48) Yao, Z. *Geometries in Soft Matter: From Geometric Frustration, Liquid Droplets to Electrostatics in Solution*; Syracuse University: Syracuse, NY, 2012.

DOI: 10.1021/acs.jpclett.9b02606
J. Phys. Chem. Lett. 2019, 10, 6375−6381